Anomalous Hall voltage rectification and quantized spin-wave excitation induced by simultaneous application of dc and rf currents in a single-layered $Ni_{81}Fe_{19}$ nanoscale wire

A. Yamaguchi,[1,2,*] K. Motoi,[1,†] A. Hirohata,[3] and H. Miyajima[1,‡]
[1]*Department of Physics, Keio University, Hiyoshi, Yokohama 223-8522, Japan*
[2]*PRESTO, JST, Honcho, Kawaguchi, Saitama 332-0012, Japan*
[3]*Department of Electronics, University of York, Heslington, York YO10 5DD, England*
(Received 5 November 2008; revised manuscript received 18 May 2009; published 8 June 2009)

An anomalous Hall effect and rectification of a Hall voltage are observed by applying a radio-frequency (rf) current through a single-layered ferromagnetic wire located on a coplanar waveguide. The components of the magnetization precession, both in and perpendicular to the plane, can be detected via the Hall voltage rectification of the rf current by incorporating an additional direct current (dc). In this paper, we propose a phenomenological model, which describes the time-dependent anisotropic magnetoresistance and the time-dependent planer Hall effect. The nonlinearity of the spin dynamics accompanied by spin waves as functions of rf currents and dc is also studied, as well as those of the magnitude and orientation of the external magnetic field.

DOI: 10.1103/PhysRevB.79.224409 PACS number(s): 72.20.My, 73.50.−h, 75.30.Ds, 72.25.Ba

I. INTRODUCTION

The understanding of spin dynamics in artificial nanomagnets is vital not only for fundamental magnetism but also for technological applications. One of the distinctive characteristics of the spin dynamics within a high-frequency region is the spin-wave (SW) excitation.[1,2] For example, the progress in magnetic recording spawns the development of smaller patterned media and a faster read-write time. Consequently, within such nanoscale ferromagnetic devices, both exchange and dipole energies contribute to the SW excitation, both of which are strongly dependent on the system geometry.[1,2] Accordingly, the SW resonance related to magnetization dynamics in a confined geometry has been intensively investigated by using Brillouin light scattering,[1–3] ferromagnetic resonance (FMR),[1,4] the time-resolved magneto-optical Kerr effect,[5,6] and the rectification effect.[7–12]

When a spin-polarized current flows through a ferromagnetic conductor, the spin angular momentum of the conduction electrons transfers to the magnetic moment with the assistance of the spin-transfer effect, consequently inducing the local magnetization precession.[13,14] Highly sensitive electrical detection of the magnetization dynamics is achieved by using such spin-transfer torque induced by a spin-polarized alternating current (ac current).[8,9] One of the most interesting discoveries is the rectification of the radio-frequency (rf) electromagnetic field, where the direct-current (dc) voltage spectrum is measured with respect to the magnetization dynamics and the magnitude of the spin-transfer torque.[8,9] The strength and direction of the spin-transfer torque are estimated by using the rectification effect in a magnetic tunneling junction. The spin-torque estimation also leads to detailed understanding of the spin dynamics induced by the interactions between conduction electrons and magnetic moments.

About 50 years ago, Juretchke[7] discovered the rectification effect and the Hall effect in a thin magnetic film in its FMR state, which is a consequence of the magnetoresistance oscillation induced by a microwave electromagnetic driving field. The FMR effect offers highly sensitive and simple detection of magnetization dynamics. In this paper, we extend and develop the method used to investigate the magnetization dynamics in nanoscale or micron-scale confined magnets, showing that the Hall voltage rectification is directly coupled with a dc current.

The propagation of electromagnetic waves through a ferromagnetic conductor raises some galvanomagnetic effects, reflecting the interactions between an electrical current and magnetization as described in the magnetoresistance and extraordinary Hall effects. The galvanomagnetic effects remarkably emerge in the vicinity of the FMR frequency and can be measured as electrical signals. We have conducted FMR studies on a single-layered $Ni_{81}Fe_{19}$ (Py) ferromagnetic wire under the simultaneous application of both dc and rf currents. The next question is what the spin torque excites when only the dc spin-polarized current is applied to the SW-excited state with an inhomogeneous spin distribution. For example, both the adiabatic spin-transfer and nonadiabatic torques have been experimentally confirmed to displace a domain wall (DW),[15–18] to excite a quantized SW,[19,20] and to induce a SW Doppler shift.[21] Further investigation into such responses offers deeper understanding of the spin dynamics correlated with the spin transport in inhomogeneous magnetization distributions.[22–25] Even so, the ground state under the presence of the dc spin current, inducing the instability of a uniformly magnetized state,[26,27] remains to be identified.

The rectification effect allows us to perform highly sensitive detection of the small friction of the spin dynamics within a nanoscale or micron-scale confined magnet. Therefore, we propose a phenomenological model for the magnetoresistance response induced by continuous-wave (CW) microwave excitation and a dc, and also present a consistent view of dc voltage generation in a ferromagnetic wire. This model is applied to the spin dynamics induced by both the dc and rf currents, which are measured as dc spectra in a well-resolved frequency domain. A perpendicular standing spin wave (PSSW) in addition to a quantized in-plane SW is detected as the rectification of the planer Hall effect (PHE). The generation of a Hall voltage signal is expected to be ex-

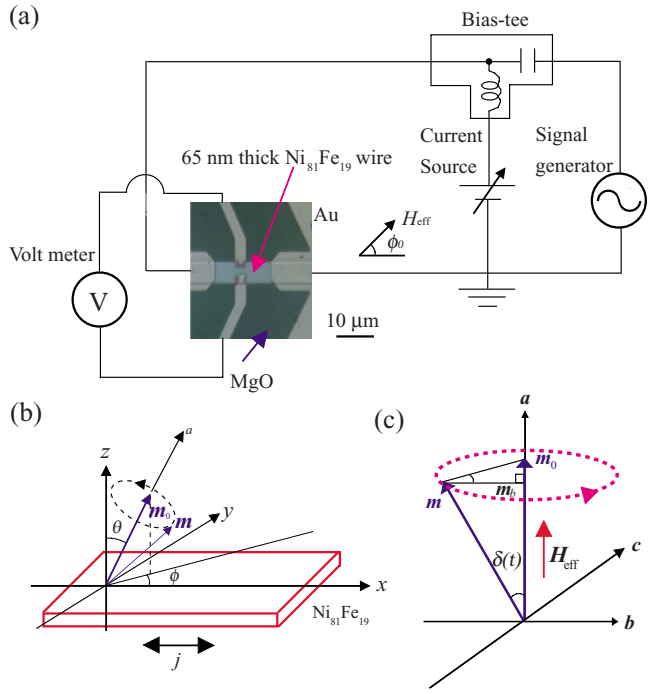

FIG. 1. (Color online) (a) Schematic of the rf measurement, including an overview of the optical micrograph of the device, and (b) the corresponding model geometry and symbol definitions. (c) Schematic projection of the magnetic-moment precession in (a,b,c) coordinate axes.

pressed as either $V_{dc+rf}^{Hall}=V_{dc}^{Hall}+V_{rf}^{Hall}$ or $V_{dc+rf}^{Hall}=V_{dc}^{Hall}+V_{rf}^{Hall}+\delta V_{dc\bullet rf}^{Hall}$, where V_{dc}^{Hall}, V_{rf}^{Hall}, and $\delta V_{dc\bullet rf}^{Hall}$ represent the dc Hall voltage, the rf Hall voltage, and the mixing term which corresponds to the additional Hall voltage induced by the coupling between the dc and rf currents.

In this paper, we present an experimental investigation on the Hall voltage rectification effect due to the magnetization dynamics in a single-layered ferromagnetic micron-scale Py wire. The present experimental setup used is presented in Sec. II, while Sec. III provides our analytical model concerning the Hall voltage based on the magnetoresistance oscillations by the combined application of both the dc and rf currents. The experimental results of the Hall voltage measured in the ferromagnetic wire are described in Sec. IV. We focus on their characteristic dependences on both the dc and the magnetic field orientation, both of which are assessed by our proposed model, while in Sec. V, the conclusions are summarized.

II. EXPERIMENTAL SETUP

A 65-nm-thick Py wire, 150 μm long and 5 μm wide, was fabricated on an epitaxially polished single-crystalline MgO(001) substrate via a combination of ultrahigh vacuum deposition, electron-beam lithography, and the lift-off method.[10] Figure 1(a) shows an optical micrograph of the wire together with an electric measurement circuit. The wire was placed on the center conductive strip line within the coplanar waveguide (CPW) structure. A sinusoidal CW rf current with a current density of 1.5×10^{10} A/m^2 was subsequently injected into the wire by a signal generator within the frequency range 10 MHz and 15 GHz. Simultaneously, a dc was applied to the above rf current via the bias tee, which separates the dc and rf components of the current. The external magnetic field $\boldsymbol{H}_{ext}$ was also applied to the substrate plane as a function of angle ϕ_0 from the major axis of the wire. The magnetization precession in the vicinity of the FMR state induced an anisotropic magnetoresistance (AMR) oscillation[7–12] and also generated the dc voltage V_{AMR}. The experiment was performed at room temperature with the slowly sweeping frequency of the rf current flowing along the major axis of the wire. The Hall voltage spectra V_{Hall}, induced across the minor axis of the wire, were also simultaneously measured.

III. ANALYTICAL MODEL

The electrical conduction in a ferromagnet generally depends on the direction of the magnetization, and the phenomenological relationship between the voltage $\boldsymbol{E}$ and the electrical current density $\boldsymbol{j}$ is written as[7]

$$\boldsymbol{E}=\rho_{\perp}\boldsymbol{j}+\boldsymbol{m}(\boldsymbol{j}\cdot\boldsymbol{m})\cdot(\rho_{\parallel}-\rho_{\perp})+\rho_H\boldsymbol{m}\times\boldsymbol{j}, \quad (1)$$

where $\boldsymbol{m}$ is the unit vector along the local magnetization, $\rho_{\perp}$ and $\rho_{\parallel}$ are the resistivities perpendicular and parallel to $\boldsymbol{j}$, respectively, and ρ_H is the extraordinary Hall resistivity. Juretschke[7] introduced an oscillating component of the magnetization $\boldsymbol{m}=\boldsymbol{m}_0+\delta\boldsymbol{m}(t)$ into Eq. (1) and pointed out that a dc voltage is generated in the magnetization precession induced by the rf electric field.

The frequency spectra of the SW excitations in a ferromagnetic wire are evaluated by using the analytical model proposed by Guslienko *et al.*[28] Using their model, in order to focus on the essence of the phenomena, we introduce a simplified phenomenological analysis based on the macrospin model, which corresponds to the SW mode with the lowest index. As shown in the coordinate system in Fig. 1(b), when the magnetization unit vector at the origin is $\boldsymbol{m}=(\sin\theta\cos\phi,\sin\theta\sin\phi,\cos\theta)$ directing along the effective magnetic field orientation and the electrical current flows along the longitudinal axis of the wire as $\boldsymbol{j}=(j(t),0,0)$, the electric field $\boldsymbol{E}$ is given by

$$\boldsymbol{E}(t)=\begin{pmatrix}E_x(t)\\E_y(t)\\E_z(t)\end{pmatrix}=j(t)\begin{pmatrix}\rho_{\perp}+\Delta\rho\sin^2\theta\cos^2\phi\\\Delta\rho\sin^2\theta\cos\phi\sin\phi+\rho_H\cos\theta\\\Delta\rho\sin\theta\cos\theta\cos\phi-\rho_H\sin\theta\sin\phi\end{pmatrix}, \quad (2)$$

where $\Delta\rho=\rho_{\parallel}-\rho_{\perp}$. Here, the current has dc and rf components, $j(t)=j_{dc}+j_{rf}\,\mathrm{Re}(e^{-i\omega t})=j_{dc}+j_{rf}\cos\omega t$, where j_{dc} and j_{rf} denote the dc and rf current densities, respectively, and ω is the angular frequency of the rf excitation current. To simplify the electric field described in Eq. (2), the magnetization is assumed to point along the effective magnetic field in the substrate plane due to the strong magnetic shape anisotropy and the external static magnetic field, namely, $\theta=90°$. When

the rf current in addition to the dc is injected into the $Ni_{81}Fe_{19}$ wire, the magnetization precession is induced by its driving torque, including the spin-transfer effect and the nonuniform magnetic field.[13,14,22–25] Consequently, the time-dependent electric fields, E_x, E_y, and E_z along the major axis (x axis), the minor axis (y axis), and the vertical axis (z axis) of the wire due to the precession are, respectively, given by

$$E_x(t) = j(t)\{\rho_\perp + \Delta\rho \cos^2[\phi + \delta(t)]\}, \tag{3}$$

$$E_y(t) = j(t)\Delta\rho \cos[\phi + \delta(t)]\sin[\phi + \delta(t)], \tag{4}$$

and

$$E_z(t) = -j(t)\rho_H \sin[\phi + \delta(t)], \tag{5}$$

where $\delta(t)$ is the magnetization precessional angle around the effective field and is generally defined so as to involve both in- and out-of-plane excursions of the magnetization, which differ significantly due to the demagnetizing-field-induced ellipticity of the magnetization precession. The individual contributions are discussed later in this section. Equations (3)–(5) indicate the AMR effect, the PHE, and the anisotropic Hall effect, respectively. By expanding Eqs. (3)–(5) using the addition formula of a trigonometric function, we can derive an average time-dependent electric field to the second order of the dynamic magnetization precessional angle $\delta(t)$ as follows:

$$E_x(t) \approx j(t)\left\{\rho_\perp + \Delta\rho\left[\cos^2\phi - \frac{1}{2}\sin 2\phi \sin 2\delta(t) - \cos 2\phi \sin^2 \delta(t)\right]\right\}, \tag{6}$$

$$E_y(t) \approx \frac{1}{2}j(t)\Delta\rho[\sin 2\phi \cos 2\phi \sin 2\delta(t) - 2 \sin 2\phi \sin^2 \delta(t)], \tag{7}$$

and

$$E_z(t) \approx -j(t)\rho_H\left[\sin\phi + \cos\phi \sin\delta(t) - \frac{1}{2}\sin\phi \sin^2\delta(t)\right]. \tag{8}$$

These relations clearly illustrate that the time variation in the electric fields $E_x(t)$, $E_y(t)$, and $E_z(t)$ is induced by the magnetization precession and the injection of the time-dependent microwave field.

To understand the phenomena qualitatively, we treat the magnetization dynamics in a simple state, where the magnetization only precesses around the effective magnetic field direction as mentioned above. The previous models are based on the assumption that the SW excitation can be described by the smooth undulation and small amplitude of the magnetization. In our present model, the Landau-Lifshitz-Gilbert (LLG) equation is considered, including the spin-transfer torque and the rf magnetic field, which consists of both an inhomogeneous electromagnetic field and a dynamic demagnetizing field due to the SW excitation. The LLG equation to describe the magnetization dynamics is therefore written by[22–25]

$$\frac{\partial \boldsymbol{m}}{\partial t} = -\gamma_0 \boldsymbol{m} \times (\boldsymbol{H}_{\text{eff}} + \boldsymbol{h}_{\text{rf}}) + \alpha \boldsymbol{m} \times \frac{\partial \boldsymbol{m}}{\partial t} - (\boldsymbol{u}\cdot\nabla)\boldsymbol{m} + \beta \boldsymbol{m} \times [(\boldsymbol{u}\cdot\nabla)\boldsymbol{m}], \tag{9}$$

where $\boldsymbol{m}(t)$ denotes the unit vector along the local magnetization ($\boldsymbol{m}=\boldsymbol{M}/M_S$, $|\boldsymbol{m}|=1$, and M_S, saturation magnetization), and γ_0, $\boldsymbol{H}_{\text{eff}}$, $\boldsymbol{h}_{\text{rf}}$, and α represent the gyromagnetic ratio, the effective magnetic field including exchange and demagnetizing fields, the rf field produced by the rf current flowing through the middle strip of the CPW, and the Gilbert damping constant, respectively. Furthermore, $\boldsymbol{u}$ is given by using the current density $\boldsymbol{j}$ and the spin polarization of the current P as follows:[21–25]

$$\boldsymbol{u} = \boldsymbol{j}\frac{P\mu_B}{eM_S}. \tag{10}$$

Here, the previous approaches have been developed based on the LLG equation, while our present treatment includes one additional important aspect; the spin-transfer torque in the SW excitation state gives the precession of the precessional axis of the magnetization itself.[29] Therefore, we introduce the angular vector $\boldsymbol{\Omega}$ and replace the time derivative of $\boldsymbol{m}(t)$ with the following:

$$\frac{\partial \boldsymbol{m}(t)}{\partial t} \Rightarrow \frac{\partial \boldsymbol{m}(t)}{\partial t} + \boldsymbol{\Omega} \times \boldsymbol{m}(t). \tag{11}$$

Consequently, Eq. (9) is rewritten as

$$\frac{\partial \boldsymbol{m}}{\partial t} + \boldsymbol{\Omega} \times \boldsymbol{m} = -\gamma_0 \boldsymbol{m} \times (\boldsymbol{H}_{\text{eff}} + \boldsymbol{h}_{\text{rf}}) + \alpha \boldsymbol{m} \times \left(\frac{\partial \boldsymbol{m}}{\partial t} + \boldsymbol{\Omega} \times \boldsymbol{m}\right) - (\boldsymbol{u}\cdot\nabla)\boldsymbol{m} + \beta \boldsymbol{m} \times [(\boldsymbol{u}\cdot\nabla)\boldsymbol{m}]. \tag{12}$$

In the right-hand side of Eqs. (9) and (12), the second term represents the damping effect, and the third and fourth terms correspond to the spin-transfer torque and spin flip of the conduction electrons, respectively.[22–25] From Eqs. (9) and (12), the magnetization gradient along the electric field $-(\boldsymbol{u}\cdot\nabla)\boldsymbol{m} + \beta \boldsymbol{m} \times [(\boldsymbol{u}\cdot\nabla)\boldsymbol{m}]$ is obtained when the spin-transfer torque and spin-flip term dominate the magnetization dynamics. The vector Eq. (12) can be linearized and projected onto the two normal vectors $\boldsymbol{b}$ and $\boldsymbol{c}$ as shown in Fig. 1(c). Here, Eq. (12) for the case of $\theta=90°$ is considered since the magnetization nearly lies in the plane and aligns along the major axis (x axis) due to the sufficiently strong magnetic shape anisotropy. In defining the present coordinate system, $\boldsymbol{b}$ is in the x-y plane and $\boldsymbol{c}$ is perpendicular to the x-y plane. Now, $\boldsymbol{m}=\boldsymbol{m}_0+\delta\boldsymbol{m}$ with $|\boldsymbol{m}|=1$, where $\boldsymbol{m}_0=(m_0,0,0)$ corresponds to the equilibrium direction of the magnetization along the effective magnetic field (a axis), and the small deviation $\delta\boldsymbol{m}(t)$ is $(0, m_b(t), m_c(t)) \approx (0, m_b e^{i\omega t}, m_c e^{i\omega t})$. The angular vector $\boldsymbol{\Omega}$ is given by $(0,0,\Omega_0)$ since the magnetization precesses in the plane, while the spin current $\boldsymbol{u}$ is con-

sidered to be spatially uniform along the longitudinal axis of the wire (x axis). With the axes defined in Fig. 1, $\boldsymbol{u}$ is given by $\boldsymbol{u}=(u(t),0,0)=(u_{\rm dc}+u_{\rm rf}\cos\omega t,0,0)$ in the (x,y,z) coordinate system. The adiabatic and nonadiabatic spin-transfer torque terms are therefore obtained in the (a,b,c) coordinate system[29] to the first order of the deviations $\delta\boldsymbol{m}(t)$,

$$-(\boldsymbol{u}\cdot\nabla)\boldsymbol{m}+\beta\boldsymbol{m}\times[(\boldsymbol{u}\cdot\nabla)\boldsymbol{m}]=u(t)\frac{\partial\phi}{\partial x}\begin{pmatrix}0\\-1\\\beta\end{pmatrix}. \quad (13)$$

Next, the dynamic and static magnetic field terms and the damping term are calculated. These terms are described as the first and second terms in the right-hand side of Eq. (12), respectively. The external magnetic field is directed at the angle ϕ_0 from the $+x$ coordinate axis. Subsequently, we redefine a new (a,b,c) coordinate system, where the $+a$ direction corresponds to the equilibrium direction of $\boldsymbol{m}_0$ along the effective magnetic field $\boldsymbol{H}_{\rm eff}=\boldsymbol{H}_{\rm ext}+\boldsymbol{H}_A$ ($\boldsymbol{H}_{\rm ext}$ is an external field and $\boldsymbol{H}_A$ is a shape anisotropy field).

The magnetization precession around $\boldsymbol{H}_{\rm eff}$ results in a small time-dependent component of the magnetization perpendicular to $\boldsymbol{m}_0$, which inclines at the angle ϕ from the $+x$ axis. The magnetic fields, $\boldsymbol{H}_{\rm eff}$, $\boldsymbol{H}_{\rm ext}$, and $\boldsymbol{H}_A$, in the (a,b,c) coordinate system satisfy the following relationship:[30]

$$\boldsymbol{H}_{\rm eff}=\boldsymbol{H}_{\rm ext}+\boldsymbol{H}_A. \quad (14)$$

Here,

$$\boldsymbol{H}_{\rm ext}=[H_{\rm ext}\cos(\phi_0-\phi),H_{\rm ext}\sin(\phi_0-\phi),0], \quad (15)$$

and

$$\boldsymbol{H}_A=-M_S\tilde{\boldsymbol{N}}\cdot\boldsymbol{m}, \quad (16)$$

where $\tilde{\boldsymbol{N}}$ is the demagnetizing-factor tensor in the (a,b,c) coordinate system, which is given by[30,31]

$$\tilde{\boldsymbol{N}}=\begin{pmatrix}N_x\cos^2\phi+N_y\sin^2\phi & \frac{1}{2}(N_x-N_y)\sin 2\phi & 0\\ \frac{1}{2}(N_x-N_y)\sin 2\phi & N_x\sin^2\phi+N_y\cos^2\phi & 0\\ 0 & 0 & N_z\end{pmatrix}, \quad (17)$$

where N_x, N_y, and N_z are the demagnetizing factors in the (x,y,z) system. It should be noted that Eq. (17) satisfies the Schlomann sum rule:[31] $\mathrm{Tr}\,\tilde{\boldsymbol{N}}=1$. Therefore, the contribution of the static magnetic field is obtained as follows:

$$-\gamma_0\boldsymbol{m}\times(\boldsymbol{H}_{\rm ext}+\boldsymbol{H}_A)\approx-\gamma_0\begin{pmatrix}-m_c e^{i\omega t}H'_{\rm eff}\\ m_c e^{i\omega t}H'_c\\ H'_{\rm eff}-m_b e^{i\omega t}H'_b\end{pmatrix}, \quad (18)$$

where

$$H'_b=H_{\rm ext}\cos(\phi_0-\phi)+M_S(N_y-N_x)\cos 2\phi, \quad (19)$$

$$H'_c=H_{\rm ext}\cos(\phi_0-\phi)+M_S[N_z-(N_x\cos^2\phi+N_y\sin^2\phi)], \quad (20)$$

and

$$H'_{\rm eff}=H_{\rm ext}\sin(\phi_0-\phi)-\frac{1}{2}M_S(N_x-N_y)\sin 2\phi. \quad (21)$$

Here, the rf field $\boldsymbol{h}_{\rm rf}$ is given by

$$\boldsymbol{h}_{\rm rf}=e^{i\omega t}(h_{\rm in}\sin\phi,h_{\rm in}\cos\phi,h_{\rm out}), \quad (22)$$

where $h_{\rm in}$ and $h_{\rm out}$ denote the in-plane and out-of-plane fields, respectively. The rf field is composed of not only the magnetic field component of the rf electromagnetic wave but also the Oersted field produced by the rf current flowing through the wire and CPW electrode.[30] Subsequently, the dynamic magnetic torque and damping terms are, respectively, obtained as follows:

$$-\gamma_0\boldsymbol{m}\times\boldsymbol{h}_{\rm rf}=e^{i\omega t}\begin{pmatrix}0\\ \gamma_0 h_{\rm out}\\ -\gamma_0 h_{\rm in}\cos\phi\end{pmatrix} \quad (23)$$

and

$$\alpha\boldsymbol{m}\times\left(\frac{\partial\boldsymbol{m}}{\partial t}+\boldsymbol{\Omega}\times\boldsymbol{m}\right)=e^{i\omega t}\begin{pmatrix}-\alpha\Omega_0 m_c\\ -i\omega\alpha m_c\\ i\omega\alpha m_b+\Omega_0\alpha e^{-i\omega t}\end{pmatrix}. \quad (24)$$

By substituting Eqs. (13), (18), (23), and (24) into Eq. (12) and neglecting the minor quadratic terms, we obtain

$$(\gamma_0 H'_{\rm eff}+\alpha\Omega_0)m_c+\Omega_0 m_b=0, \quad (25)$$

and

$$\begin{pmatrix}i\omega & [\gamma_0 H'_c+i\omega\alpha]\\ -[\gamma_0 H'_b+i\omega\alpha] & i\omega\end{pmatrix}\begin{pmatrix}m_b\\ m_c\end{pmatrix}=e^{-i\omega t}\begin{pmatrix}-\Omega_0-u_{\rm dc}\frac{\partial\phi}{\partial x}\\ \alpha\Omega_0+\beta u_{\rm dc}\frac{\partial\phi}{\partial x}\end{pmatrix}+\gamma_0\begin{pmatrix}h_{\rm out}\\ -h_{\rm in}\cos\phi\end{pmatrix}+u_{\rm rf}\frac{\partial\phi}{\partial x}\begin{pmatrix}-1\\ \beta\end{pmatrix}. \quad (26)$$

The component m_b is obtained by solving Eq. (26),

$$m_b=\frac{1}{\det|\chi|}\{e^{-i\omega t}[i\omega A_1-(\gamma_0 H'_c+i\omega\alpha)B_1]+[i\omega A_2-(\gamma_0 H'_c+i\omega\alpha)B_2]\}, \quad (27)$$

where the driving terms A_1, B_1, A_2, B_2, and $\det|\chi|$ are, respectively, given by

$$A_1=-\Omega_0-u_{\rm dc}\frac{\partial\phi}{\partial x}, \quad (28)$$

$$B_1 = \alpha\Omega_0 + \beta u_{\rm dc}\frac{\partial\phi}{\partial x}, \tag{29}$$

$$A_2 = \gamma_0 h_{\rm out} - u_{\rm rf}\frac{\partial\phi}{\partial x}, \tag{30}$$

$$B_2 = -\gamma_0 h_{\rm in}\cos\phi + \beta u_{\rm rf}\frac{\partial\phi}{\partial x}, \tag{31}$$

$$\det|\chi| = -\omega^2 + [\gamma_0 H_c' + i\omega\alpha]\cdot[\gamma_0 H_b' + i\omega\alpha], \tag{32}$$

and the FMR frequency ω_k and full width at half maximum $\Delta\alpha$ are written by

$$\omega_k^2 = \gamma_0^2 H_c' H_b' \tag{33}$$

and

$$\Delta\alpha = \gamma_0(H_b' + H_c')\alpha. \tag{34}$$

Taking the complex conjugates into account, the m_b in the FMR state is derived as

$$m_b(t) = D_0 + D_1\cos\omega_k t + D_2\sin\omega_k t, \tag{35}$$

where the coefficients D_0, D_1, and D_2 are given by the following relations, respectively:

$$D_0 = \frac{A_1 - B_1}{\alpha\Delta} = -\frac{1}{\alpha\Delta}\left[\Omega_0(1+\alpha) + (1+\beta)u_{\rm dc}\frac{\partial\phi}{\partial x}\right], \tag{36}$$

$$D_1 = \frac{A_2 - \alpha B_2}{\alpha\Delta} = \frac{1}{\alpha\Delta}\left[\gamma_0(h_{\rm out} + \alpha h_{\rm in}\cos\phi) - (1+\alpha\beta)u_{\rm rf}\frac{\partial\phi}{\partial x}\right], \tag{37}$$

and

$$D_2 = -\frac{\gamma_0 H_c'}{\omega_k\alpha\Delta}B_2 = -\frac{\gamma_0 H_c'}{\omega_k\alpha\Delta}\left(-\gamma_0 h_{\rm in}\cos\phi + \beta u_{\rm rf}\frac{\partial\phi}{\partial x}\right). \tag{38}$$

The first term in the right-hand side of Eq. (35) describes the magnetization precession due to the dc spin-transfer effect, while the second and last terms show the in-phase and out-of-phase driving torque, respectively. The space derivative term $\partial\phi/\partial x$ is introduced as a phenomenological parameter of the spin-transfer terms. The individual components of the effective field, including the demagnetizing factor of the wire, H_b', H_c', and $H_{\rm eff}'$, are derived in Eqs. (19)–(21), respectively, which correspond to the terms described in our previous paper.[30] The adequately small precessional angle $\delta(t)$ is given by $\boldsymbol{m}$, and $\delta\boldsymbol{m}(t)$ satisfies $\sin\delta(t) \approx \langle\sqrt{m_b^2 + m_c^2}\rangle/|\boldsymbol{m}|$. The out-of-plane component m_c generates the dynamic demagnetizing field and exerts torque proportional to $\boldsymbol{m}\times\delta\boldsymbol{m}$ onto the magnetization, rotating $\boldsymbol{m}$ by the angle $\delta(t)$ in the plane.

The usual uniform mode analysis leads to an estimation of an ellipticity

$$\eta = \frac{|m_c|}{|m_b|}. \tag{39}$$

The value is obtained by the H_b' and H_c' parameters which may be viewed as effective stiffness fields, charactering the instantaneous torque exerted on the magnetization $\boldsymbol{m}$ which is tipped parallel or perpendicular to the driving torque direction, respectively. The ellipticity η is estimated to be about 0.23 by using the relation $\sqrt{H_b'/H_c'}$ (when $\phi \approx \phi_0 = 45°$, $N_x \approx 0$, $N_y \approx 0.05$, and $N_z \approx 0.95$). The explicit dependence of the value η of the external magnetic field $H_{\rm ext}$ on the field angle ϕ_0 for the resonance at a given frequency ω_k can also be determined. Meanwhile, the relationship between m_b and m_c as described in Eq. (25) provides the estimation of the contribution toward the ellipticity η due to the spin-transfer effect, only if the spin torque dominates the FMR excitation. The contribution is estimated to be about 0.1 because the damping constant α of $Ni_{81}Fe_{19}$ is typically 0.01, $\gamma_0 H_{\rm eff}' \approx 734$ MHz (when $\phi \approx \phi_0 = 45°$, $N_x \approx 0$, $N_y \approx 0.05$, and $N_z \approx 0.95$) as estimated by Eq. (21) and Ω_0 is also estimated to be $\omega_k \approx 6.3$ GHz corresponding to the FMR frequency given by Eq. (33).[1,2,28,30,32] These results indicate that the magnetization precesses around the effective-field direction with a highly elliptical orbit in the plane. According to Eq. (39), $\delta(t)$ satisfies

$$\sin\delta(t) \approx \frac{m_b\sqrt{1+\eta^2}}{|\boldsymbol{m}|} = m_b\sqrt{1+\eta^2} \quad \text{and} \quad \sin 2\delta(t) \approx 2m_b\sqrt{1+\eta^2}. \tag{40}$$

Following the substitution of Eqs. (35) and (40) into Eqs. (6)–(8), the time variation in the individual electric fields $E_x(t)$, $E_y(t)$, and $E_z(t)$ is calculated. Here, in the FMR state ($\omega = \omega_k$), the experimentally measured voltages are given by the time average of $\langle E_x(t)\rangle$, $\langle E_y(t)\rangle$, and $\langle E_z(t)\rangle$. As $\langle\cos^2\omega t\rangle = \langle\sin^2\omega t\rangle = 1/2$, the time-independent voltages are given by

$$\langle E_x(t)\rangle \approx j_{\rm dc}\left[\rho_\perp + \Delta\rho\cos^2\phi - \sqrt{1+\eta^2}D_0\Delta\rho\sin 2\phi - (1+\eta^2)\left(D_0^2 + \frac{D_1^2 + D_2^2}{2}\right)\Delta\rho\cos 2\phi\right] - j_{\rm rf}\left[\frac{\Delta\rho}{2}\sqrt{1+\eta^2}D_1\sin 2\phi - (1+\eta^2)D_0 D_1\cos 2\phi\right], \tag{41}$$

$$\langle E_y(t)\rangle \approx \frac{1}{2}j_{\rm dc}\Delta\rho\left[\sin 2\phi + 2\sqrt{1+\eta^2}D_0\cos 2\phi - 2(1+\eta^2)\left(D_0^2 + \frac{D_1^2+D_2^2}{2}\right)\sin 2\phi\right]$$
$$+ \frac{1}{2}j_{\rm rf}\Delta\rho[\sqrt{1+\eta^2}D_1\cos 2\phi - 2(1+\eta^2)D_0D_1\sin 2\phi], \quad (42)$$

and

$$\langle E_z(t)\rangle \approx j_{\rm dc}\rho_H\left[\sin\phi + \sqrt{1+\eta^2}D_0\cos\phi - \frac{1}{2}(1+\eta^2)\left(D_0^2 + \frac{D_1^2+D_2^2}{2}\right)\sin\phi\right] + \frac{1}{2}j_{\rm rf}\rho_H[\sqrt{1+\eta^2}D_1\cos\phi - (1+\eta^2)D_0D_1\sin\phi], \quad (43)$$

By substituting Eqs. (36)–(38) into Eqs. (41) and (42), the field angle ϕ_0 dependence of the individual variations in the rectified signals is obtained when the magnetization aligns almost parallel to $\boldsymbol{H}_{\rm ext}$ under the condition $|\boldsymbol{H}_{\rm ext}| \gg |\boldsymbol{H}_A|$, namely, $\phi_0 \approx \phi$. Here, if there is a uniform spin structure in the wire, its variation with x is negligible and hence the spin torque does not play an important role. Then, the spin dynamics under the spin torque does not occur along the x direction. In other words, $\Omega_0=0$, which means $D_0 \approx 0$. In previous studies, Eqs. (41)–(43) are approximated to the first order of D_1, and only the rectifying voltage in combination with the rf current and magnetization dynamics are under consideration.

Here, the second order of $D_n(n=0,1,2)$ should be reserved since the second terms of the right-hand side in Eqs. (41)–(43) provide interplaying contributions between the dc $j_{\rm dc}$ and the rf current $j_{\rm rf}$. These terms cannot be negligible when both the dc and rf currents are simultaneously applied. Although these terms provide only minute contributions to the dc voltage spectra, they still play an important role in distinguishing individual contributions of the various driving torques as shown in Sec. IV D.

For example, the magnetization dynamics induced by the in-plane rf field $h_{\rm in}$ due to the microwave introduction (i.e., $j_{\rm dc}=0$ and $j_{\rm rf}\neq 0$) gives the amplitude of the dc voltages, $V_{\rm AMR}(\omega_k)$ and $V_{\rm Hall}(\omega_k)$ by Eqs. (41) and (42) in the FMR state, corresponding to the AMR voltage generated along the major (x) axis and the Hall voltage induced along the minor (y) axis as follows:

$$\Delta V_{\rm AMR}(\omega_k, I_{\rm dc}=0\ \text{mA}) \propto \sin 2\phi\cos\phi, \quad (44)$$

$$\Delta V_{\rm Hall}(\omega_k, I_{\rm dc}=0\ \text{mA}) \propto \cos 2\phi\cos\phi. \quad (45)$$

IV. EXPERIMENTAL RESULTS AND DISCUSSION

A. Simultaneous measurement of the voltages generated along the major and minor axes without dc current

First, the rectification spectra generated along the x and y axes are simultaneously measured without applying a dc, so as to confirm whether anomalous behaviors are produced by the microwave distribution. An example of representative spectra without the dc at $H_{\rm ext}=500$ Oe and $\phi=45°$ is shown in Fig. 2(a), where the voltage amplitude in the FMR state is defined as a peak-to-peak value as shown in the figure. The angle ϕ dependence of $\Delta V_{\rm AMR}$ and $\Delta V_{\rm Hall}$ is shown in Figs. 2(b) and 2(c) together with the curve fitted with Eqs. (44) and (45). As is seen in the figure, the ϕ dependence in the case of a low field ($H_{\rm ext}=100$ Oe) does not seem to agree with the calculation, since the uniform precession is difficult to be realized when the magnetization is not directed along the low external field. Bailleul *et al.*[33] reported that the nonzero y component of the exchange field proportional to d^2M_y/dx^2 is attributed to a noncollinear magnetization alignment in the vicinity of the edge. This leads to the departure of the angular dependences of $\Delta V_{\rm AMR}$ and $\Delta V_{\rm Hall}$ from the analytical fitting curve. Conversely, where $H_{\rm ext}=500$ Oe exceeding the shape anisotropy field, the curve fitting with Eqs.

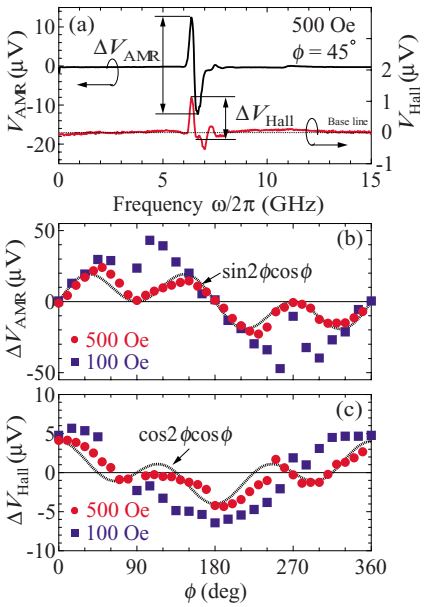

FIG. 2. (Color online) (a) Typical rectifying AMR and Hall spectra in the absence of the dc current measured under the external static field of 500 Oe at $\phi=45°$. The amplitudes of both $\Delta V_{\rm AMR}$ and $\Delta V_{\rm Hall}$ are defined as the voltage difference between the peak and dip in the FMR frequency. (b) $\Delta V_{\rm AMR}$ and (c) $\Delta V_{\rm Hall}$ as a function of the field angle ϕ under $H_{\rm ext}=100$ [(blue) solid squares] and 500 Oe [(red) solid circles]. Fitting lines with Eqs. (44) and (45) are also shown.

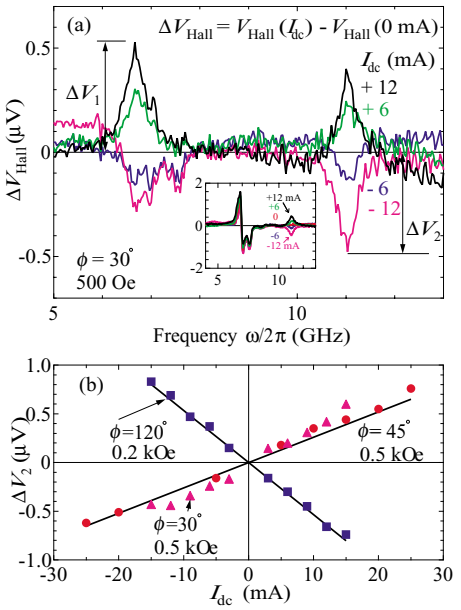

FIG. 3. (Color online) (a) Typical Hall voltage difference ΔV_{Hall} spectra, given by $\Delta V_{\mathrm{Hall}}=V_{\mathrm{Hall}}(I_{\mathrm{dc}})-V_{\mathrm{Hall}}(0\ \mathrm{mA})$, measured under $H_{\mathrm{ext}}=500$ Oe at $\phi=30°$. The inset shows the entire Hall voltage V_{Hall} spectra. (b) The dc dependence of the Hall voltage difference ΔV_2.

(44) and (45) virtually corresponds to the measured data for the uniform mode (black dotted lines).[10,30,34] Thus the spin dynamics of the nanowire under the application of dc and rf currents can be understood through the Hall voltage rectification effect as discussed below.

B. Additional Hall voltage induced by the application of the dc current

The inset of Fig. 3(a) shows the rf frequency dependence of the output signal V_{Hall} for the dc currents from $I_{\mathrm{dc}}=-12$ to +12 mA at every 6 mA in $H_{\mathrm{ext}}=500$ Oe at $\phi=30°$. The sense of the dc is defined as positive along the $+x$ direction. For clarity, the nonresonant background signal exceeding the resonant signal is subtracted. As shown in the inset of Fig. 3(a), the spectrum for $I_{\mathrm{dc}}=0$ (red solid line) has at least two distinct modes near 6.8 and 7.5 GHz, while the spectrum for $I_{\mathrm{dc}}=\pm 12$ mA has an additional distinct mode near 11.0 GHz. Figure 3(a) shows the variation in the rectified Hall signal,

$$\Delta V_{\mathrm{Hall}}(\omega_k, I_{\mathrm{dc}}) = V_{\mathrm{Hall}}(I_{\mathrm{dc}}) - V_{\mathrm{Hall}}(I_{\mathrm{dc}} = 0\ \mathrm{mA}) = V_{\mathrm{base\ line}} + \Delta V_{1(2)}. \quad (46)$$

$V_{\mathrm{base\ line}}$ and $\Delta V_{1(2)}$ represent the baseline voltage and the resonant Hall voltage difference, respectively. We focus on the I_{dc} dependence of the peak height at $\omega_k/2\pi=11$ GHz. As shown in Fig. 3(b), the peak height is proportional to I_{dc} as expected for a conventional resistive effect. In other words, the Hall voltage difference ΔV_2 is expressed by $\Delta V_2 = \Delta R_{\mathrm{PHE}} I_{\mathrm{dc}}$, where ΔR_{PHE} is the planer Hall resistance. The estimated ΔR_{PHE} is 0.032 mΩ for $\phi=45°$ and $|\boldsymbol{H}_{\mathrm{ext}}|=0.5$ kOe, and −0.053 mΩ for $\phi=120°$ and $|\boldsymbol{H}_{\mathrm{ext}}|=0.2$ kOe. It should be noted that both the sense and magnitude of ΔR_{PHE} strongly correlate with the direction of the magnetization and the precessional angle. The latter relationship between ΔR_{PHE} and the precessional angle is discussed in Sec. IV D.

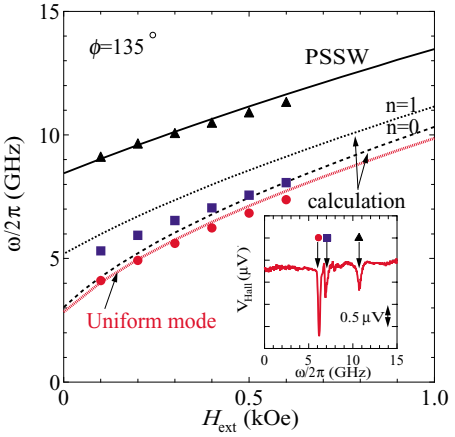

FIG. 4. (Color online) Magnetic field dependence of the resonant frequency observed by the Hall voltage spectra. The lines show the calculations as described in Ref. 28 for the quantized SW mode with quantized indices $n=0$ (black dashed line) and 1 (black dotted line), as well as the uniform mode [(red) broken line] and the PSSW mode with the lowest quantized number (black solid line labeled PSSW). (Red) circles, (blue) squares, and black triangles represent the experimental results of three peaks in the Hall voltage spectrum as typically shown in the inset.

C. Excited spin-wave modes

The magnetic field dependence of the SW frequency for each spin mode is shown in Fig. 4. All observed modes are attributed to the magnetic excitations as discussed above. In particular, the two modes observed in the lower-frequency region correspond to the quantized SW modes derived from the dipole-dipole interaction (red circles) and the dipole-exchange coupling (blue squares) due to the confined structure as discussed by Guslienko *et al.*[28] Another mode in the higher-frequency region is the PSSW mode[1,2,35] (black triangles). An empirical expression describing the complete SW modes with the quantized integer numbers is evaluated below.

According to Guslienko *et al.*[28] and Bayer *et al.*,[2] the frequency of the quantized SW modes (or eigenmodes) of a strip can be evaluated from the solution of the LLG equation and is given by

$$\left(\frac{\omega_n}{\omega_M}\right)^2 = \left(\frac{\omega_H}{\omega_M} + 1 + \frac{\lambda_n}{4\pi}\right)\left(\frac{\omega_H}{\omega_M} + Aq_{\parallel}^2 - \frac{\lambda_n}{4\pi}\right), \quad (47)$$

where A is the exchange stiffness coefficient, $q_{\parallel}$ is the in-plane wave vector, $\omega_H=\gamma_0 H_{\mathrm{ext}}$, $\omega_M=\gamma_0 4\pi M_S$, and the dipole eigenvalue λ_n is precisely given by Eq. (4) and approximately by the analytical expression of Eq. (12) as derived from Ref. 28.

In this case, an infinitely long magnetic strip is assumed, whose cross section is a rectangular of thickness d and width

w with $p=d/w \ll 1$. The SW is quantized along the width direction due to the dipole-dipole interaction under the pinning condition given by Eq. (8) in Ref. 28. This provides $q_{\parallel}=n\pi/w_{\text{eff}}$, where the integer n is the quantization number and w_{eff} is the effective wire width including the pinning effect at the edge of the strip.

The frequency variation in the PSSW mode with the applied field is qualitatively understood in terms of the rectangular cross-sectional strip. Accordingly to Kalinikos and Slavin,[1,2,35] the dispersion relationship of the SW in a confined magnetic structure is given by

$$\omega^2 = \gamma^2\left(H + \frac{2A}{M_S}q^2\right)\left(H + \frac{2A}{M_S}q^2 + 4\pi M_S F_{pp}(q_{\parallel}d_{\text{eff}})\right), \tag{48}$$

where

$$q^2 = q_x^2 + q_y^2 + \left(\frac{m\pi}{d_{\text{eff}}}\right)^2 = q_{\parallel}^2 + q_{\perp}^2, \tag{49}$$

and d_{eff} is the effective thickness for the SW wavelength including the boundary conditions given by Eq. (8) in Ref. 28, m represents the quantized number for the SW along the thickness direction, and $F_{pp}(q_{\parallel}d)$ describes the matrix element of the magnetic-dipole interaction.[35]

The comparison between the experimental results and the analytical SW eigenfrequencies estimated from Eqs. (47) and (48) for the two lowest modes ($n=0$ and 1) and another mode ($m=1$) is presented in Fig. 4. These results imply that the above analytical calculations explain our present results very well. Consequently, the effective width w_{eff} and thickness d_{eff} are estimated to be 5.2 μm and 65 nm, respectively, both of which are almost equivalent to the measured width and thickness of the strip. This clearly indicates that the quantized SW is excited under the edge or surface pinning conditions. To simplify the rectification spectrum, the phenomenological macrospin model as described by Eq. (9) is introduced, and the validity of the introduction of the uniform mode corresponding to the lowest quantized SW mode ($n=0$ and $m=0$) is examined. As shown in Fig. 4, the calculation of Eq. (32) qualitatively agrees with our present results of the field angle ϕ dependence of ΔV_{AMR} and ΔV_{Hall}.

D. Angle dependence of the additional Hall voltage due to the PSSW mode induced by the dc current

As seen in Figs. 3(a) and 4, the spectra present at least three peaks centered around 6.2, 7.0, and 11.0 GHz. As discussed above, these frequencies are derived from the quantized SW. The rectangular Py strip essentially has the quantized SW modes in both lateral and horizontal directions. The two lower-frequency SW modes correspond to the quantized SW modes in the lateral direction, and the highest-frequency SW mode is the PSSW mode in the horizontal direction, respectively. In particular, the difference between the resonance frequency of the two former SW modes with the quantized indices $n=0$ and 1 is too small to be distinguished from the measurement of the angle dependence of the Hall voltage rectification spectra. Since the highest-frequency SW mode does not overlap with the other modes, it is easily discussed and treated as an outcome of the macrospin dynamics as described by Eq. (9).

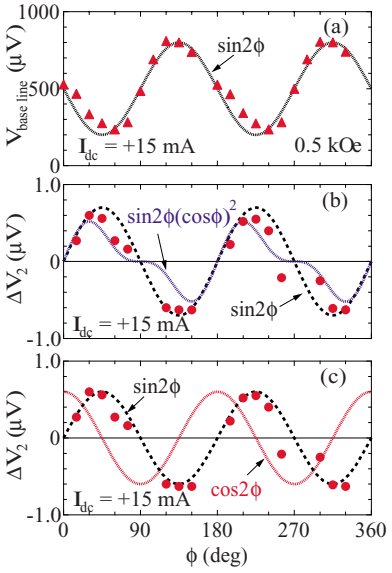

FIG. 5. (Color online) Magnetic field angle ϕ dependence of (a) the (nonresonant) baseline Hall voltage $V_{\text{base line}}$ and [(b) and (c)] the Hall voltage difference ΔV_2 induced by $I_{\text{dc}}=+15$ mA at the PSSW frequency under $H_{\text{ext}}=500$ Oe. The (black) dashed, (blue) dotted, and (red) broken lines correspond to the fitting $\sin 2\phi$, $\sin 2\phi(\cos\phi)^2$, and $\cos 2\phi$ lines derived from each contribution, respectively.

The dc voltage difference induced by the dc current, ΔV_{Hall}, given by Eq. (46) is plotted as a function of the applied magnetic field angle ϕ in Fig. 5. By using the subsequent relationship from Eqs. (42) and (46),[36] ΔV_{Hall} is written as

$$\Delta V_{\text{Hall}}(\omega_k, I_{\text{dc}}) = \frac{1}{2}I_{\text{dc}}\Delta R\left[\sin 2\phi - 2(1+\eta^2)\times\left(D_0^2 + \frac{D_1^2+D_2^2}{2}\right)\sin 2\phi - 2D_0\sqrt{1+\eta^2}\cos 2\phi\right]. \tag{50}$$

The first term in Eq. (50) corresponds to the nonresonant baseline voltage $V_{\text{base line}}=(I_{\text{dc}}\Delta R \sin 2\phi)/2$. From the second and third terms, the Hall voltage difference and the planer Hall resistance are given by

$$\Delta V_2 = -I_{\text{dc}}\Delta R\left[(1+\eta^2)\left(D_0^2 + \frac{D_1^2+D_2^2}{2}\right)\sin 2\phi + D_0\sqrt{1+\eta^2}\cos 2\phi\right] \tag{51}$$

and

$$\Delta R_{\mathrm{PHE}} = \Delta R\left[(1+\eta^2)\left(D_0^2 + \frac{D_1^2 + D_2^2}{2}\right)\sin 2\phi + D_0\sqrt{1+\eta^2}\cos 2\phi\right]. \quad (52)$$

From Eqs. (36)–(38) and (51), the voltage amplitude ΔV_2, induced by the magnetization dynamics in the PSSW mode, depends on $\sin 2\phi$, $\sin 2\phi(\cos\phi)^2$, $\sin 2\phi \cos\phi$, or $\cos 2\phi$. In addition, the sense of the ΔV_2 is opposite to that of $V_{\mathrm{base\ line}}$. The applied field angle ϕ dependence of ΔV_2 is influenced by the in-plane field, out-of-plane field, adiabatic and nonadiabatic spin torques. The out-of-plane field provides a $\sin 2\phi$ contribution, while the in-plane driving field generates either $\sin 2\phi(\cos\phi)^2$ or $\sin 2\phi \cos\phi$ contribution. The adiabatic and nonadiabatic spin torques along the major (x) axis produce $\sin 2\phi$ and $\cos 2\phi$ contributions, respectively. These predictions are confirmed by measuring the angle ϕ dependence of ΔV_2.

Figure 5(a) shows the variation in the nonresonant background baseline voltage $V_{\mathrm{base\ line}}$ for $I_{\mathrm{dc}}=+15$ mA. The excellent agreement between the experimental data and the $\sin 2\phi$ fitting curve confirms that the voltage $V_{\mathrm{base\ line}}$ is derived from the time-independent first term of the right-hand side in Eq. (50) and that the dragging effects hardly affect the spin dynamics due to the noncollinear alignment of the magnetization,[33] encouraging us to treat the spin dynamics using the macrospin model.

The experimental angle ϕ dependence of ΔV_2 is shown in Figs. 5(b) and 5(c). As expected, the sense of ΔV_2 is opposite to that of $V_{\mathrm{base\ line}}$. The (black) dashed and (blue) dotted lines shown in Fig. 5(b) correspond to the $\sin 2\phi$ and $\sin 2\phi(\cos\phi)^2$ curves, respectively. The former is derived from the out-of-plane field contribution, while the latter corresponds to the in-plane field contribution. Conversely, the (black) dashed and (red) dotted lines shown in Fig. 5(c) are calculated based on the rf and dc spin torques including the adiabatic and nonadiabatic terms. As seen in Figs. 5(b) and 5(c), the present angle ϕ dependence of ΔV_2 seems to be in agreement with the $\sin 2\phi$ fitting curve rather than the $\sin 2\phi(\cos\phi)^2$ and $\cos 2\phi$ curves. This present result demonstrates the positive agreement between our analytical calculation and experiment. At this stage, however, it is difficult to distinguish experimentally between the rf fields and spin torques, since both the rf fields and spin torques include the same angle ϕ dependence of ΔV_2 which is proportional to $\sin 2\phi$.

Further evaluation of each contribution is important to reveal the physical origin of the additional Hall voltage induced by the dc current. Initially, ΔR is estimated at 0.08 Ω from the result shown in Fig. 5(a) by using the relation $V_{\mathrm{base\ line}}=\frac{1}{2}I_{\mathrm{dc}}\Delta R \sin 2\phi$. By using the parameters, $\phi=45°$ and $\Delta R_{\mathrm{PHE}}=0.032$ mΩ in Fig. 3(b), the amplitude $D_0^2 + \frac{D_1^2+D_2^2}{2}$ is determined to be 2×10^{-2}.

The static magnetic fields due to the dc current $I_{\mathrm{dc}}=15$ mA flowing through the wire and the CPW electrodes are estimated to be $h_{\mathrm{in\text{-}plane}}^{\mathrm{static}}=\frac{I}{2w}\approx 18.8$ Oe and $h_{\mathrm{out\text{-}of\text{-}plane}}^{\mathrm{static}}=\frac{I}{2y}\approx 1.88$ Oe (Ref. 37), respectively. The static field induced by the dc current, $h_{\mathrm{in\text{-}plane}}^{\mathrm{static}}$, has additional significant effects on the field distribution and the magnetization dynamics. Consequently, the dynamic distribution of the in-plane and out-of-plane dynamic demagnetizing fields is distorted by the dc current, the magnitude of which is assumed to be $h_{\mathrm{in\text{-}plane}}\approx h_{\mathrm{out\text{-}of\text{-}plane}}\approx 1$ Oe. The out-of-plane field is calculated to be $\frac{\gamma_0 h_{\mathrm{out\text{-}of\text{-}plane}}}{\alpha\Delta}=9.3\times10^{-3}$, whereas the in-plane fields are $\frac{\alpha\gamma_0 h_{\mathrm{in\text{-}plane}}}{\alpha\Delta}=9.3\times10^{-5}$ and $\frac{\gamma_0 H_c' \gamma_0 h_{\mathrm{in\text{-}plane}}}{\omega_k \alpha\Delta}=4.3\times10^{-2}$.

On the other hand, $\partial\phi/\partial x$ from the precessional angle of the uniform mode in the 10-μm-long ferromagnetic wire is estimated to be $\frac{5°}{10\ \mu\mathrm{m}}=0.87\times10^4$ rad/m in the SW-excited state.[38] Then the spin-torque term derived from the spatial magnetization distribution $\partial\phi/\partial x$ is estimated for the following case: $\gamma_0=2.8$ MHz/Oe, $\Delta=30$ GHz, $\omega_k=6.3$ GHz, $\gamma_0 H_c'=29$ GHz, $\alpha=0.01$, $u_{\mathrm{dc}}=2.26$ m/s, and $u_{\mathrm{rf}}=0.7$ m/s, corresponding to $I_{\mathrm{dc}}=15$ mA and $I_{\mathrm{rf}}=4.8$ mA by assuming $\beta=0$ and $P=0.7$.[39] Accordingly, the adiabatic spin-transfer torques are given by $u_{\mathrm{dc}}\frac{1}{\alpha\Delta}\frac{\partial\phi}{\partial x}=6.5\times10^{-5}$ and $u_{\mathrm{rf}}\frac{1}{\alpha\Delta}\frac{\partial\phi}{\partial x}=2.0\times10^{-5}$. It is appropriate to compare each contribution with the amplitude $D_0^2+\frac{D_1^2+D_2^2}{2}$. As a result, the amplitude of the spin-transfer torque is smaller than that of the rf field even when $h_{\mathrm{in\text{-}plane}}\approx h_{\mathrm{out\text{-}of\text{-}plane}}\approx 1$ Oe. Therefore, the additional Hall voltage induced by the dc current is ascribed to the dynamic field distorted by the dc current.[40]

The present Hall voltage method offers a highly sensitive detection of the spin dynamics induced by the rf current. In addition, the existence of the mixing term $\delta V_{\mathrm{dc\bullet rf}}^{\mathrm{Hall}}$ is observed. This represents the fact that the individual contributions of the driving torque are distinguished by using our proposed method. Our technique opens a new path to understand the instabilities of microscopic ferromagnetism under spin-current flow.[21,26,27]

V. CONCLUSION

Highly sensitive measurements on dc planer Hall voltage spectra in a micron-scale single-layered $Ni_{81}Fe_{19}$ strip were performed as functions of a frequency, an external static field, a field direction, and a dc. Dynamic change in the rectification spectrum by the dc was clearly measured. Based on our phenomenological analytical model proposed, the changes produced by the inhomogeneous magnetic distributions under the coexistence of the dc current and the spin torque were quantitatively evaluated. This highly sensitive detection of microscopic spin dynamics via the planer Hall rectification effect represents a powerful technique for studying the spin dynamics within a single nanoscale or micron-scale confined magnetic structure. Our technique provides a way to understand the detailed correlation between a localized magnetic moment and a conduction electron.

ACKNOWLEDGMENTS

The present study was partly supported by MEXT Grants-in-Aid for Scientific Research in a Priority Area and a JSPS Grants-in-Aid for Scientific Research. A.Y. also acknowledges support from the JST PRESTO program.

APPENDIX: DETAILED SOLUTION OF THE LLG EQUATION

In our approach, magnetization dynamics are solved by Eq. (12). The details of each term in Eq. (12) are defined as follows:

$$\frac{d\boldsymbol{m}}{dt} + \boldsymbol{\Omega} \times \boldsymbol{m} = e^{i\omega t}\begin{pmatrix} -\Omega_0 m_b \\ i\omega m_b + \Omega_0 e^{-i\omega t} \\ i\omega m_c \end{pmatrix}, \tag{A1}$$

$$\begin{aligned} &-\gamma_0 \boldsymbol{m} \times (\boldsymbol{H}_{\text{ext}} + \boldsymbol{H}_A) \\ &\approx -\gamma_0 \begin{pmatrix} -m_c e^{i\omega t} H_{\text{ext}} \sin(\phi_0 - \phi) \\ m_c e^{i\omega t} H_{\text{ext}} \cos(\phi_0 - \phi) \\ H_{\text{ext}} \sin(\phi_0 - \phi) - m_b e^{i\omega t} H_{\text{ext}} \cos(\phi_0 - \phi) \end{pmatrix} \\ &-\gamma_0 \begin{pmatrix} m_c e^{i\omega t} \frac{1}{2} M_S (N_x - N_y) \sin 2\phi \\ m_c e^{i\omega t} M_S [N_z - (N_x \cos^2 \phi + N_y \sin^2 \phi)] \\ -\frac{1}{2} M_S (N_x - N_y) \sin 2\phi - m_b e^{i\omega t} (N_y - N_x) \cos 2\phi \end{pmatrix} \\ &= -\gamma_0 \begin{pmatrix} -m_c e^{i\omega t} H'_{\text{eff}} \\ m_c e^{i\omega t} H'_c \\ H'_{\text{eff}} - m_b e^{i\omega t} H'_b \end{pmatrix}, \end{aligned} \tag{A2}$$

$$-\gamma_0 \boldsymbol{m} \times \boldsymbol{h}_{\text{rf}} = e^{i\omega t}\begin{pmatrix} 0 \\ \gamma_0 h_{\text{out}} \\ -\gamma_0 h_{\text{in}} \cos \phi \end{pmatrix}, \tag{A3}$$

$$\alpha \boldsymbol{m} \times \left(\frac{d\boldsymbol{m}}{dt} + \boldsymbol{\Omega} \times \boldsymbol{m} \right) = e^{i\omega t}\begin{pmatrix} -\alpha \Omega_0 m_c \\ -i\omega \alpha m_c \\ i\omega \alpha m_b + \Omega_0 \alpha e^{-i\omega t} \end{pmatrix}. \tag{A4}$$

In the (x,y,z) coordinate system, the spin-polarized current directed along the x axis is given by $\boldsymbol{u} = \frac{P\mu_B}{eM_S} j(1,0,0)$. The unit vector along the effective field is described by $\boldsymbol{m} = (\sin\theta\cos\phi, \sin\theta\sin\phi, \cos\theta)$. Subsequently, the adiabatic and nonadiabatic spin-transfer torque terms are, respectively, derived as

$$\begin{aligned} -(\boldsymbol{u}\cdot\nabla)\boldsymbol{m} &= -\frac{P\mu_B}{eM_S} j \cdot \frac{\partial}{\partial x}\begin{pmatrix} \cos\phi \\ \sin\phi \\ 0 \end{pmatrix} \\ &= -\frac{P\mu_B}{eM_S} j \cdot \begin{pmatrix} -\sin\phi \frac{\partial \phi}{\partial x} \\ \cos\phi \frac{\partial \phi}{\partial x} \\ 0 \end{pmatrix} \end{aligned} \tag{A5}$$

and

$$\beta \boldsymbol{m} \times [(\boldsymbol{u}\cdot\nabla)\boldsymbol{m}] = \frac{\beta P \mu_B}{eM_S} j \begin{pmatrix} 0 \\ 0 \\ \frac{\partial \phi}{\partial x} \end{pmatrix}. \tag{A6}$$

Both spin-torque terms in the (a,b,c) coordinate system can be obtained by a rotation transformation from the (x,y,z) coordinate system to the (a,b,c) coordinate system,

$$-(\boldsymbol{u}\cdot\nabla)\boldsymbol{m} = -\frac{P\mu_B}{eM_S} j \begin{pmatrix} 0 \\ \frac{\partial \phi}{\partial x} \\ 0 \end{pmatrix} \tag{A7}$$

and

$$\beta \boldsymbol{m} \times [(\boldsymbol{u}\cdot\nabla)\boldsymbol{m}] = \beta \frac{P\mu_B}{eM_S} j \begin{pmatrix} 0 \\ 0 \\ \frac{\partial \phi}{\partial x} \end{pmatrix}. \tag{A8}$$

*yamaguch@phys.keio.ac.jp
†kmotoi@phys.keio.ac.jp
‡miyajima@phys.keio.ac.jp

[1] B. Hillebrands and K. E. Ounadjela, *Spin Dynamics in Confined Magnetic Structures* (Springer, Berlin, 2003), Vol. 1-3.
[2] C. Bayer, J. Jorzick, B. Hillebrands, S. O. Demokritov, R. Kouba, R. Bozinoski, A. N. Slavin, K. Y. Guslienko, D. V. Berkov, N. L. Gorn, and M. P. Kostylev, Phys. Rev. B **72**, 064427 (2005); S. O. Demokritov, B. Hillebrands, and A. N. Slavin, Phys. Rep. **348**, 441 (2001).
[3] A. Ercole, A. O. Adeyeye, J. A. C. Bland, and D. G. Hasko, Phys. Rev. B **58**, 345 (1998).
[4] M. Bailleul, R. Höllinger, and C. Fermon, Phys. Rev. B **73**, 104424 (2006).
[5] A. Barman, V. V. Kruglyak, R. J. Hicken, J. M. Rowe, A. Kundrotaite, J. Scott, and M. Rahman, Phys. Rev. B **69**, 174426 (2004).
[6] M. Belov, Z. Liu, R. D. Sydora, and M. R. Freeman, Phys. Rev. B **69**, 094414 (2004).
[7] H. J. Juretschke, J. Appl. Phys. **31**, 1401 (1960); W. M. Moller

and H. J. Juretschke, Phys. Rev. B **2**, 2651 (1970).
[8] A. A. Tulapurkar, Y. Suzuki, A. Fukushima, H. Kubota, H. Maehara, K. Tsunekawa, D. D. Djayaprawira, N. Watanabe, and S. Yuasa, Nature (London) **438**, 339 (2005); H. Kubota, A. Fukushima, K. Yakushiji, T. Nagahama, S. Yuasa, K. Ando, H. Maehara, Y. Nagamine, K. Tsunekawa, D. D. Djayaprawire, N. Watanabe, and Y. Suzuki, Nat. Phys. **4**, 37 (2008).
[9] J. C. Sankey, P. M. Braganca, A. G. F. Garcia, I. N. Krivorotov, R. A. Buhrmann, and D. C. Ralph, Phys. Rev. Lett. **96**, 227601 (2006); J. C. Sankey, Y.-T. Cui, J. Z. Sun, J. C. Slonczewski, R. A. Burhrman, and D. C. Ralphs, Nat. Phys. **4**, 67 (2008).
[10] A. Yamaguchi, H. Miyajima, T. Ono, Y. Suzuki, and S. Yuasa, Appl. Phys. Lett. **90**, 182507 (2007); A. Yamaguchi, H. Miyajima, S. Kasai, and T. Ono, *ibid.* **90**, 212505 (2007); A. Yamaguchi, H. Miyajima, T. Ono, Y. Suzuki, and S. Yuasa, *ibid.* **91**, 132509 (2007).
[11] M. V. Costache, M. Sladkov, C. H. van der Wal, and B. J. van Wees, Appl. Phys. Lett. **89**, 192506 (2006); M. V. Costache, S. M. Watts, M. Sladkov, C. H. van der Wal, and B. J. van Wees, *ibid.* **89**, 232115 (2006).
[12] Y. S. Gui, N. Mecking, X. Zhou, Gwyn Williams, and C.-M. Hu, Phys. Rev. Lett. **98**, 107602 (2007); N. Mecking, Y. S. Gui, and C. M. Hu, Phys. Rev. B **76**, 224430 (2007).
[13] J. C. Slonczewski, J. Magn. Magn. Mater. **159**, L1 (1996).
[14] L. Berger, Phys. Rev. B **54**, 9353 (1996).
[15] P. P. Freitas and L. Berger, J. Appl. Phys. **57**, 1266 (1985); C. Y. Hung and L. Berger, *ibid.* **63**, 4276 (1988).
[16] A. Yamaguchi, T. Ono, S. Nasu, K. Miyake, K. Mibu, and T. Shinjo, Phys. Rev. Lett. **92**, 077205 (2004).
[17] G. S. D. Beach, C. Knutson, C. Nistor, M. Tsoi, and J. L. Erskine, Phys. Rev. Lett. **97**, 057203 (2006).
[18] M. Kläui, P.-O. Jubert, R. Allenspach, A. Bischof, J. A. C. Bland, G. Faini, U. Rüdiger, C. A. F. Vaz, L. Vila, and C. Vouille, Phys. Rev. Lett. **95**, 026601 (2005).
[19] M. Tsoi, A. G. M. Jansen, J. Bass, W.-C. Chiang, V. Tsoi, and P. Wyder, Nature (London) **406**, 46 (2000).
[20] Y. Ji, C. L. Chien, and M. D. Stiles, Phys. Rev. Lett. **90**, 106601 (2003).
[21] V. Vlaminck and M. Bailleul, Science **322**, 410 (2008).
[22] L. Berger, J. Appl. Phys. **49**, 2156 (1978); **55**, 1954 (1984).
[23] G. Tatara and H. Kohno, Phys. Rev. Lett. **92**, 086601 (2004).
[24] S. Zhang and Z. Li, Phys. Rev. Lett. **93**, 127204 (2004).
[25] A. Thiaville, Y. Nakatani, J. Miltat, and Y. Suzuki, Europhys. Lett. **69**, 990 (2005).
[26] J. Shibata, G. Tatara, and H. Kohno, Phys. Rev. Lett. **94**, 076601 (2005).
[27] Y. Nakatani, J. Shibata, G. Tatara, H. Kohno, A. Thiaville, and J. Miltat, Phys. Rev. B **77**, 014439 (2008).
[28] K. Yu. Guslienko, S. O. Demokritov, B. Hillebrands, and A. N. Slavin, Phys. Rev. B **66**, 132402 (2002).
[29] A. Thiaville and Y. Nakatani, J. Appl. Phys. **104**, 093701 (2008).
[30] A. Yamaguchi, K. Motoi, A. Hirohata, H. Miyajima, Y. Miyashita, and Y. Sanada, Phys. Rev. B **78**, 104401 (2008).
[31] E. Schlomann, J. Appl. Phys. **33**, 2825 (1962).
[32] K. Perzlmaier, G. Woltersdorf, and C. H. Back, Phys. Rev. B **77**, 054425 (2008).
[33] M. Bailleul, D. Olligs, and C. Fermon, Phys. Rev. Lett. **91**, 137204 (2003).
[34] A. Yamaguchi, K. Motoi, H. Miayajima, and Y. Nakatani, J. Appl. Phys. **105**, 07D301 (2009).
[35] B. A. Kalinikos and A. N. Slavin, J. Phys. C **19**, 7013 (1986).
[36] Here, the amplitude of the dc voltages, $V_{\mathrm{AMR}}(\omega_k)$ and $V_{\mathrm{Hall}}(\omega_k)$, is calculated by using Eqs. (41) and (42) by replacing both the current density j and the resistivity ρ with the current I and resistance R, respectively.
[37] These values are obtained by substituting the width of the wire ($w=5$ μm) and the distance between the center conductive line and ground line ($y=50$ μm).
[38] For precise analysis, accurate estimation of the derivatives $\frac{\partial\phi}{\partial x}$, $\frac{\partial\phi}{\partial y}$, $\frac{\partial\theta}{\partial x}$, and $\frac{\partial\theta}{\partial y}$ is important. However, as the SW length and the amplitude of the SW modes cannot be explicitly defined in the measurements, the derivatives are difficult to determine precisely at this stage. On the other hand, the derivatives $\frac{\partial\phi}{\partial y}$ and $\frac{\partial\theta}{\partial y}$ dominate the higher-order SW excitation state as described by Eq. (47), where the two-dimensional spin variation contains a large DW or higher-order SW excitation.
[39] J. Bass, W. P. Pratt, Jr., J. Magn. Magn. Mater. **200**, 274 (1999).
[40] Similar effect can be expected in a microscopic ferromagnetic structure with the presence of a DW. If a twisted spin structure such as DW existed in the wire, the contributions of the spin torques may also increase with the spatial derivatives. For instance, the contributions of the driving torques can be evaluated in a twisted spin structure of 180° DW with 300 nm in width. $\frac{\partial\phi}{\partial x}$ is estimated to be $\frac{180^\circ}{300\ \mathrm{nm}}=1.05\times10^7$ rad/m. The contribution of the adiabatic spin-transfer torque is $u_{\mathrm{dc}}\frac{1}{\alpha\Delta}\frac{\partial\phi}{\partial x}=7.9\times10^{-2}$ and $u_{\mathrm{rf}}\frac{1}{\alpha\Delta}\frac{\partial\phi}{\partial x}=2.5\times10^{-2}$, indicating that the spin torque controls the magnetization dynamics. These values are much larger than the additional Hall voltage induced by the dc current and hence are not applicable to our results here. Similarly, $\partial\phi/\partial y$ can be obtained for the higher-order SW excitation, which is hard to describe using the one-dimensional spin-configuration model.